Phytomedicine 122 (2024) 155108

Contents lists available at ScienceDirect

Phytomedicine

journal homepage: www.elsevier.com/locate/phymed

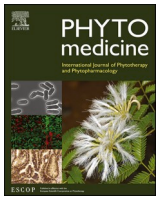

Original Article

Aloe vera peel-derived nanovesicles display anti-inflammatory properties and prevent myofibroblast differentiation

Orlando Ramírez [a,1], Florencia Pomareda [a,1], Belén Olivares [b], Ya-Lin Huang [a], Gabriela Zavala [a], Javiera Carrasco-Rojas [a], Simón Álvarez [a], Camila Leiva-Sabadini [c], Valeria Hidalgo [a], Pablo Romo [a], Matías Sánchez [a], Ayleen Vargas [a], Jessica Martínez [a], Sebastian Aguayo [c,d], Christina M.A.P. Schuh [a,*]

[a] *Centro de Medicina Regenerativa, Facultad de Medicina, Clínica Alemana- Universidad del Desarrollo, Santiago, Chile*
[b] *Centro de Química Medica, Facultad de Medicina, Clínica Alemana-Universidad del Desarrollo, Santiago, Chile*
[c] *Institute for Biological and Medical Engineering, Schools of Engineering, Medicine and Biological Sciences, Pontificia Universidad Católica de Chile, Santiago, Chile*
[d] *Dentistry School, Faculty of Medicine, Pontificia Universidad Católica de Chile, Santiago, Chile*

ARTICLE INFO

Keywords:
Plant extracellular vesicles
Nanotherapy
Interkingdom communication

ABSTRACT

Background: Aloe vera (AV) is a medicinal plant, most known for its beneficial effects on a variety of skin conditions. Its known active compounds include carbohydrates and flavonoids such as quercetin and kaempferol, among others. In the past decade, plant nanovesicles (NVs) have gained considerable interest as interkingdom communicators, presenting an opportunity for clinical standardization of natural products. In this study, we aimed to assess the potential of AVpNVs for the treatment of burn wounds.

Methods: AVpNVs were isolated and characterized regarding vesicle yield (nanoparticle tracking analysis) and structure (transmission electron microscopy and atomic force microscopy), as well as their protein content with proteomics. We assessed key characteristics for treating burn wounds *in vitro,* such as the anti-inflammatory potential in LPS-stimulated macrophages and keratinocytes, and the effect of AVpNVs on myofibroblast differentiation and contraction.

Key findings: AVpNVs presented a homogenous NV population, vesicular shape, and NV-associated protein markers. AVpNVs significantly decreased the secretion of pro-inflammatory cytokines TNFα, IL-1β, and IL-6. Furthermore, AVpNVs inhibited myofibroblast differentiation and significantly decreased their contractile potential in collagen matrices. Observed effects were linked to proteins identified in the isolates through proteomics analysis.

Conclusion: AVpNVs displayed characteristics as an inflammatory modulator, while simultaneously diminishing myofibroblast differentiation and contraction. Novel strategies for burn wound treatment seek to decrease scarring on a cellular and molecular level in the early stages of wound healing, which makes AVpNVs a promising candidate for future plant-vesicle-based treatments.

Abbreviations: AFM, atomic force microscopy; ANOVA, analysis of variance; αSMA, alpha smooth muscle actin; AVp, *Aloe vera* peel; BCA, bicinchoninic acid protein assay; BrdU, bromodeoxyuridine; DMEM, Dulbecco's Modified Eagle Medium; NV, nanovesicle; FBS, fetal bovine serum; H4, Histone 4; HDNF, Human dermal neonatal fibroblasts; HPLC, High Performance Liquid Chromatography; HSP70, heat shock protein 70; IL, Interleukin; KAE, kaempferol; LPA, lysophosphatidic acid; LPS, lipopolysaccharide; NTA, nanoparticle tracking analysis; PBS, phosphate buffered saline; PFA, paraformaldehyde; pfPBS, particle-free phosphate buffered saline; PLL, poly-L-lysine; QCT, quercetin; RIPA, radioimmunoprecipitation assay buffer; SD, standard deviation; SOD, superoxide dismutase; TEM, transmission electron microscopy; TGF, transforming growth factor; TNF, Tumor Necrosis Factor.

* Corresponding author.
E-mail address: cschuh@udd.cl (C.M.A.P. Schuh).
[1] These authors contributed equally to this work.

https://doi.org/10.1016/j.phymed.2023.155108
Received 3 May 2023; Received in revised form 30 August 2023; Accepted 19 September 2023
Available online 21 September 2023

Introduction

Burn wounds are a complex medical issue, with 8.9 million people per yr requiring medical attention due to burn injuries (James et al., 2020). The associated treatment is among the most expensive for traumatic wounds, due to long recovery times and extensive scar treatment (Sánchez et al., 2007). Hypertrophic scars, displaying a raised and contracted appearance, are a main issue in burn wounds and affect up to 67% of patients (Bijlard et al., 2017; Bombaro et al., 2003). On a cellular level, these scars contain high amounts of parallel-orientated type III collagen and myofibroblasts responsible for tissue contraction (Slemp and Kirschner, 2006). Until today, the underlying mechanisms of excessive hypertrophic scarring remain elusive, however, several mechanisms have been identified. Among those are excessive and persistent local inflammation (Wang et al., 2020), alterations in growth factor secretion (increased secretion of TGF-β1,-2,-3, bFGF and VEGF in keratinocytes (Wang et al., 2011; Xue et al., 2000)) and alterations in cellular apoptosis, such as the failure of myofibroblasts to undergo apoptosis (Moulin et al., 2004) (summarized by Penn et al. 2012). Therefore, novel treatments seek to control hyper-inflammation in the early stages, and as a consequence, reduce hypertrophic scar formation.

In this sense, extracellular vesicles (EVs) have gained considerable interest in the last decade. EVs are nanoscale membranous particles that contain a complex biological cargo, secreted by e.g. mammalian, plant or insect cells, and are able to modulate biological processes (Agrahari et al., 2019; Hade et al., 2022). EVs have been shown to be key players in cellular communication, and moreover, in interkingdom communication. Recently, several groups have demonstrated that EVs isolated from plants – called nanovesicles (NVs)- resemble the medicinal properties associated to the plant of origin. Among those are for example lemon NVs, *Aloe saponaria* NVs or cabbage NVs displaying anti-inflammatory properties (Kim and Park, 2022; Raimondo et al., 2022; You et al., 2021) or Turmeric-derived NVs alleviating colitis ulcerosa (Gao et al., 2022), as well as citrus NVs inhibiting cancer growth (Raimondo et al., 2015).

Aloe vera is a well-known natural remedy to treat skin rashes and burn wounds that has been extensively studied in recentyr. Systematic reviews concluded an overall beneficial effect of *Aloe vera* on burn wound healing (Burusapat et al., 2018; Maenthaisong et al., 2007). Kim et al. (2021) assessed the therapeutical potential of NVs derived from *Aloe vera* peels and concluded that their antioxidant activity and migratory stimulation on dermal fibroblast and keratinocytes are suitable for chronic wound treatment. However, the active components within *Aloe vera* peel-derived NVs (AVpNVs) and their effects on cellular responses associated with burn wounds remain unknown.

Therefore, the aim of this study was to analyze AVpNVs, and to assess their potential to reduce the secretion of pro-inflammatory cytokines, to inhibit myofibroblast differentiation as well as to diminish their contractile capacity, and therefore act as a novel therapeutical approach against scar formation in burn wounds.

Materials and methods

Extended and detailed methods are available in the supplemental material

AVpNV enrichment and characterization

EVs were isolated as previously described with some modifications (Kim et al., 2021). Briefly, *Aloe vera* leaves were rinsed with distilled water, cut in half, and mucilage was removed. Subsequently, the peels were chopped and incubated in phosphate buffered saline (PBS) for 1 h at room temperature. Peel residues were separated with a strainer and the soluble fraction was cleared by serial centrifugation at 500xg for 10 min, 1.000xg for 10 min, 1.750xg for 15 min and 2.500xg for 25 min (Hermle, GmbH, Germany). The resulting supernatant was filtered through 0.22 μm filters and ultracentrifuged at 100.000xg for 70 min (Hanil 5, fixed rotor, Korea). Finally, the pellet containing AVpNVs was resuspended in particle-free PBS (pfPBS) and stored at −80 °C until further use.

Protein quantification

Protein concentration in AVpNVs samples was measured with bicinchoninic acid protein assay kit (BCA kit, Thermo Fisher, USA) following the manufacturer's instruction.

Particle quantification with nanoparticle tracking analysis (NTA)

Particle concentration and size distribution were measured using a NanoSight 300 (Malvern, UK). For this, samples were diluted 1:100 with pfPBS and injected into the system using an automatic pump. Three 20 s videos were captured with a camera level 14 and measured with a detection threshold 5. Sample volume in experiments was normalized by particle concentration in the range 30–150 nm.

Analysis of AVpNV morphology

To verify vesicle structure, transmission electron microscopy (TEM) and atomic force microscopy (AFM) were employed. For TEM, AVpNV samples were placed on formvar/carbon-coated copper meshes (size 300, Ted Pella Inc.) for 15 s, counterstained with uranyl acetate for 1 min and dried at room temperature (Schuh et al., 2019). AVpNVs were visualized on a Thermo Fisher Talos Microscope.

For AFM, AVpNVs were immobilized on freshly cleaved mica discs (12 mm diameter; Electron Microscopy Sciences, USA) coated with 0.1 M solution of poly-L-lysine (PLL, Sigma Aldrich, USA), previously described (Leiva-Sabadini et al., 2021). Samples were analyzed with an Asylum MFP 3D-SA AFM (Asylum Research, US) in intermittent contact mode (AC mode) with TAP300GD-G cantilevers (BudgetSensors, Bulgaria), obtaining height, amplitude, and phase channel images of substrates.

Quantification of total carbohydrate content

Carbohydrate content of isolated AVpNV samples and pre-isolation AVp extracts were measured with a "Total Carbohydrate Assay Kit" (Sigma Aldrich, US) according to manufactureŕs instructions.

Quantification of total phospholipid content

Phospholipid content of isolated AVpNV samples and pre-isolation AVp extracts was quantified using a "Total Lipid Assay Kit" (Sigma Aldrich, US) according to manufactureŕs instructions.

Quantification of quercetin and kaempferol

High Performance Liquid Chromatography (HPLC) analysis was performed for the two flavonoids quercetin and kaemperol, as described by Colombo et al. (2017).

Anti-inflammatory effects of AVpNVs

For all cell culture assays, cells were cultivated under standard cell culture conditions at 37 °C and with 5% CO_2 in a humidified incubator. Standard medium for HaCat and Human dermal neonatal fibroblasts was based on Dulbecco's Modified Eagle Medium (DMEM, Gibco, US), and for THP-1 cells RPMI1640, all supplemented with 200 mM l-glutamine and 1% (v/v) penicillin-streptomycin (Sigma, US) and varying amounts of fetal bovine serum (FBS; indicated for each assay).

The anti-inflammatory potential of AVpNVs was assessed in two macrophage cell lines stimulated with LPS and keratinocytes stimulated with LPS, analyzing the subsequent secretion of pro-inflammatory cytokines. All three cell types (Raw264.7, THP-1 M0 phenotype, HaCat) were cultured with their respective standard medium supplemented with 10% FBS (HyClone, GE Healthcare, USA) until 70% confluency, and split with accutase (Thermo Fisher). Cells were seeded at a density of 1.25×10^4 cells/cm^2 in 12-well plates and left to adhere overnight. AVpNVs were added to the medium at a ratio 100 or 500 NVs per cell 8 h prior to stimulation and 20 μg/ml indomethacin (a non-steroidal anti-inflammatory drug) 2 h prior to stimulation with 1 μM LPS (Fig. 3A).

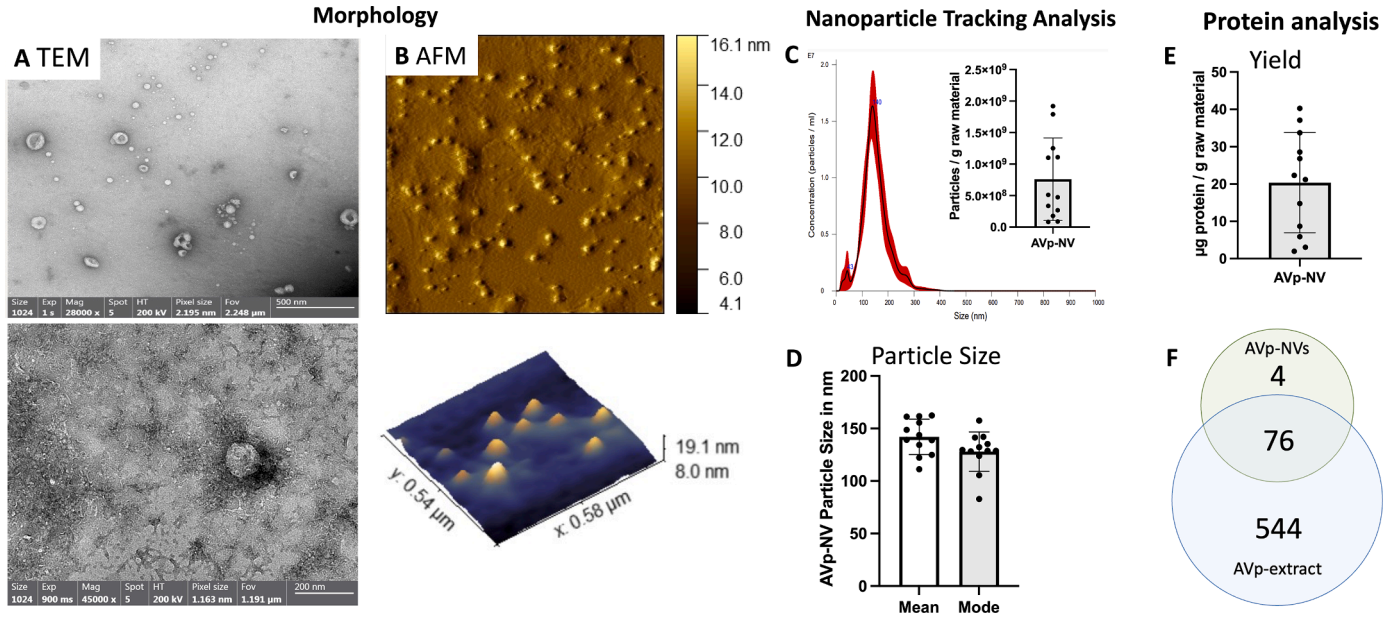

Fig. 1. AVpNVs characterization: (A) representative TEM images of AVpNVs, scale bar shows 500 nm and 200 nm; $n = 3$; (B) AFM characterization of AVpNVs, $n = 3$; (/D) AVpNV particle analysis: representative NTA histogram with particle yield normalized to gram of raw material (inlay) (C) and analysis of particle size-mean and mode (D); $n = 12$; (E). protein yield normalized by grams of raw material; $n = 12$; Data is displayed as mean ± SD. (F) Venn diagram of proteins identified with proteomics in AVpNVs and AVp extract.

Supernatant was collected after 24 h LPS-stimulation and centrifuged at 1.500xg for 15 min to remove cellular debris and stored at −80 °C until further use. Cells from each well were counted for subsequent normalization. Tumor Necrosis Factor alpha (TNFα), Interleukin 1 beta (IL-1β) and Interleukin 6 (IL-6) were quantified with sandwich ELISA (DuoSet, R&D Systems) according to manufacturer's instructions. Results were normalized to 100.000 cells, based on the cell count after LPS stimulation.

Effect of AVpNVs on myofibroblast differentiation

Human dermal neonatal fibroblasts (HDNF, Thermo Fisher, USA) were seeded at a density of 5.2×10^3 cells/cm^2. After 24 h incubation in full media with 10%FBS, cells were washed with PBS and starved with 0.3% FBS for 24 h. HDNF were differentiated into myofibroblasts with transforming growth factor beta1 (TGFβ1, R&D system, USA) (0.5 ng/ml, 72 h) in full media with 2.5% FBS. AVpNVs were added at a ratio of 100 or 500 NVs per cell. For subsequent Western Blot analysis, proteins were isolated with RIPA buffer (Sigma Aldrich, USA). Differentiation was assessed with α-smooth muscle actin (α-SMA) expression. Briefly, proteins were separated in a 10% acrylamide gel, blotted onto a nitrocellulose membrane and after blocking, incubated with primary antibody overnight (Cell Signaling, US; αSMA #19245; GAPDH #2118). Subsequently, membranes were revealed and analyzed with the Odyssey CLx imaging system.

Confocal microscopy

After 48 h of cultivation, cells fixed in paraformaldehyde, permeabilized and blocked with 1% BSA for 30 min. Cells were stained with primary antibody rabbit anti-αSMA, washed with PBS, and incubated with secondary antibody anti-rabbit Alexa Fluor® 555, along with 0.2 µM Alexa Fluor™ 488 phalloidin, for 60 min. Nuclei were stained with 8 µM Hoechst33342 for 5 min. Samples were visualized with Fluoview FV10i confocal microscope (Olympus, Shinjuku, Japan).

Collagen contraction assay

To assess the contractile potential of HDNF and myofibroblasts in the presence of AVpNVs, a collagen contraction assay was utilized. Myofibroblasts were differentiated from HDNF as described above. For collagen gels, a type I collagen solution (2 mg/mL in hydrochloric acid; Gibco, USA) was mixed with 10x MEM (Gibco, USA) in a ratio of 8:1. After neutralization, HDNF or myofibroblasts were added at a concentration of 1.5×10^6 cells/mL, together with AVpNVs at a ratio of 100 or 500 NVs per cell (Fig. 5A). Hydrogels with respective cells but without AVpNVs, with 10 µM lysophosphatidic acid (LPA, Sigma; positive control) and 10 µM Y27632 (Sigma; negative control) served as controls. The mixture was transferred to a 96-well plate (100 µl/well) and incubated at 37 °C for 60 min to allow gelation. Subsequently, gels were detached from the well using a sterile needle and covered with standard medium supplemented with 5% FBS. After 24 h macroscopic images were taken of each gel, and collagen area was measured with ImageJ software (NIH, USA). The percentage of gel contraction was calculated with the following formula:

$$\%\ collagen\ contraction\ = \left(\frac{Well\ area - \ Collagen\ gel\ area}{Well\ area}\right) * 100$$

Statistics

All data are presented as mean +/- standard deviation (SD). Normality was tested with Shapiro-Wilk test. N values were defined as independent AVpNVs isolations and independent experiments. Statistical difference between two groups was assessed with student *t*-test, for three and more groups with one-way ANOVA followed by Tukey's post-hoc test. Significance was considered $p < 0.05$ and specific values are reported in figure legends. Analysis was performed using GraphPad Prism 9 for Mac OS X, version 9.3.2 (GraphPad software, Inc).

Results

AVpNV characterization

Aloe vera (*Aloe barbadensis miller*) was characterized with HPLC (Supplemental Fig. 4). AVpNVs were enriched through ultracentrifugation and characterized in terms of morphology, size, particle concentration, and protein concentration. AVpNVs exhibited a round shape consistent with the morphology of EVs (Fig. 1A and B). Total particle concentration was $6.5 \pm 5.7 \times 10^8$ particles/gram of raw material

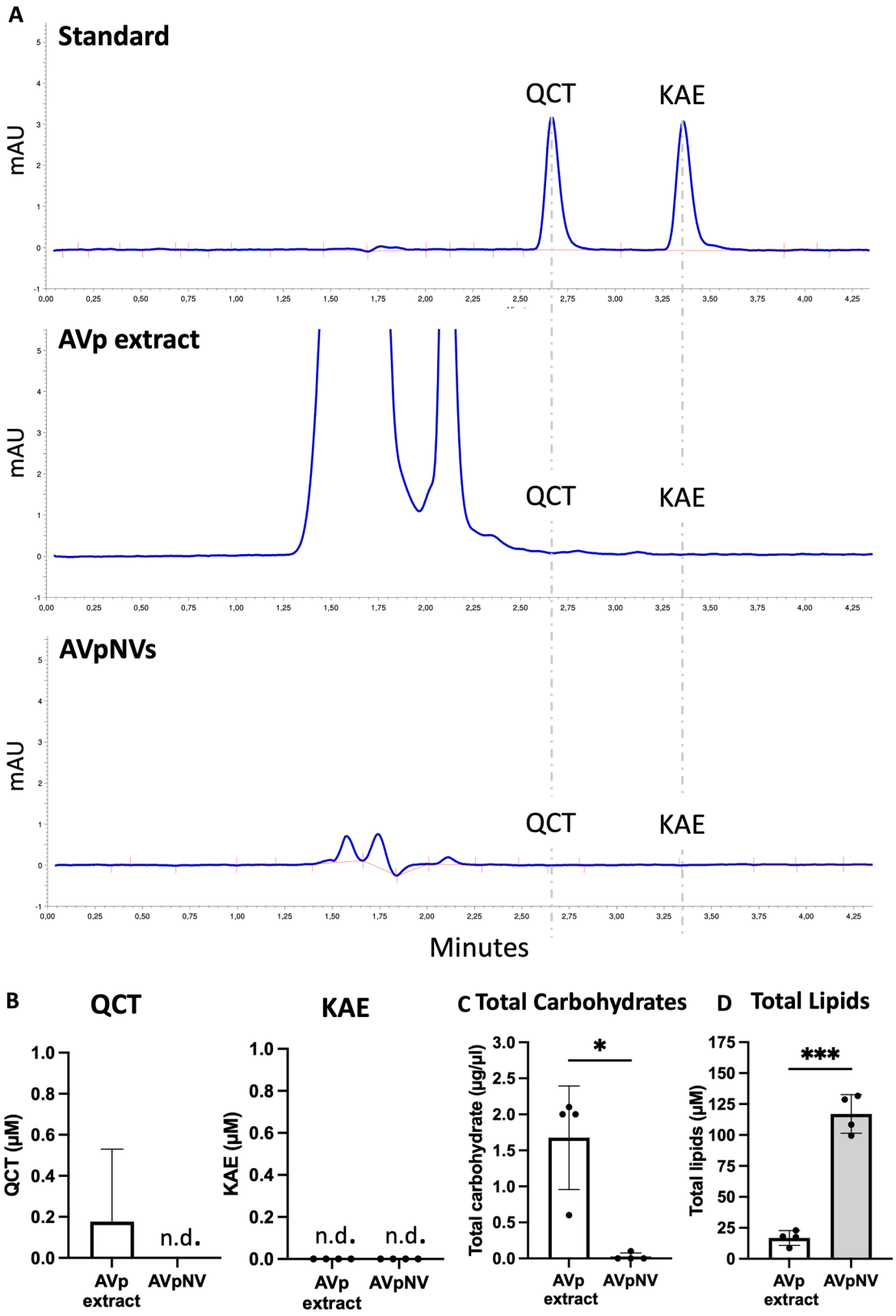

Fig. 2. Analysis of AVpNV isolates; (A/B) HPLC analysis of isolated AVpNVs compared to pre-isolation supernatant (AVp extract); A) representative chromatograms of quercetin (QCT) and kaempferol (KAE) standards, AVp extract and AVpNVs, and (B) quantification of quercetin and kaempferol in AVp extract and AVpNVs; n.d. = not detected; Data is displayed as mean ± SD, $n = 4$; (C) Quantification of total carbohydrates, isolated AVpNVs compared to pre-isolation AVp extract; results shown as µg/µl $n = 4$; (D) Quantification of total lipids, isolated AVpNVs compared to pre-isolation AVp extract; results shown µM of total lipids; data are displayed as mean ± SD, $n = 4$. *$p < 0.05$, **$p < 0.01$, ***$p < 0.001$, ****$p < 0.0001$.

Table 1
List of proteins identified with liquid chromatography – tandem mass spectrometry from AVpNVs.

Protein	Length	Protein description
tr|A0A5P1EEM4|A0A5P1EEM4_ASPOF	220	14–3–3 domain-containing protein
tr|A0A2H9ZV19|A0A2H9ZV19_9ASPA	263	14–3–3-like protein
tr|A0A2I0×313|A0A2I0×313_9ASPA	267	14–3–3-like protein B
tr|A0A2I0ATR1|A0A2I0ATR1_9ASPA	261	14–3–3-like protein D
tr|A0A2I0VRD7|A0A2I0VRD7_9ASPA	250	14–3–3-like protein GF14 kappa
tr|F8UCF0|F8UCF0_ALLCE	238	33 kDa manganese stabilizing chloroplast protein (Fragment)
tr|A0A5P1E582|A0A5P1E582_ASPOF	150	40S ribosomal protein S14
tr|A0A5P1FCN6|A0A5P1FCN6_ASPOF	152	40S ribosomal protein S18
tr|A0A5P1FHL3|A0A5P1FHL3_ASPOF	109	40S ribosomal protein S25
tr|A0A2I0A1D4|A0A2I0A1D4_9ASPA	65	40S ribosomal protein S28
tr|A0A0A7LYU1|A0A0A7LYU1_ALBBR	235	40S ribosomal protein S3–3-like protein
tr|A0A2I0AWP2|A0A2I0AWP2_9ASPA	226	40S ribosomal protein S8
tr|A0A2I0WM50|A0A2I0WM50_9ASPA	227	40S ribosomal protein S8
tr|A0A5P1ES47|A0A5P1ES47_ASPOF	777	5-methyltetrahydropteroyltriglutamate–homocysteine S-methyltransferase
tr|A0A2I0ATM4|A0A2I0ATM4_9ASPA	94	60S ribosomal protein L37a
tr|G3KF67|G3KF67_NARTA	377	Actin
tr|A0A0A7LUI4|A0A0A7LUI4_ALBBR	376	Actin 7 isoform 1
sp|P0DTE7|AMY1B_HUMAN	511	Alpha-amylase 1B
tr|A0A5P1FT59|A0A5P1FT59_ASPOF	253	Aspergillus nuclease S1
tr|A0A2H9ZTT6|A0A2H9ZTT6_9ASPA	379	ATP synthase gamma chain, chloroplastic
tr|A0A5C0CJP8|A0A5C0CJP8_9ASPA	507	ATP synthase subunit alpha, chloroplastic
tr|A0A835PZY0|A0A835PZY0_VANPL	524	ATP synthase subunit beta
tr|A0A6G7KYP5|A0A6G7KYP5_9ASPA	498	ATP synthase subunit beta, chloroplastic
tr|A0A5P1FTZ3|A0A5P1FTZ3_ASPOF	481	Beta-glucosidase
tr|A0A5P1F4I6|A0A5P1F4I6_ASPOF	224	Chlorophyll a-b binding protein, chloroplastic
tr|A0A240EY31|A0A240EY31_ALOMC	83	Cytochrome b559 subunit alpha
tr|A0A5P1ET91|A0A5P1ET91_ASPOF	293	Elongation factor 1-alpha
tr|A0A8T3BBI6|A0A8T3BBI6_DENNO	389	Fructose-bisphosphate aldolase
tr|A0A8T3A8×3|A0A8T3A8×3_DENNO	162	Glutaredoxin-dependent peroxiredoxin
sp|P09211|GSTP1_HUMAN	210	Glutathione S-transferase P
tr|A0A5P1E3S0|A0A5P1E3S0_ASPOF	204	Glyceraldehyde 3-phosphate dehydrogenase NAD(P) binding domain-containing protein
tr|A0A2I0AJS0|A0A2I0AJS0_9ASPA	341	Glyceraldehyde-3-phosphate dehydrogenase
tr|J7FRA3|J7FRA3_9ASPA	264	Glyceraldehyde-3-phosphate dehydrogenase (Fragment)
tr|A0A2I0B5S7|A0A2I0B5S7_9ASPA	651	Heat shock cognate 70 kDa protein
tr|A0A0A7LUI9|A0A0A7LUI9_ALBBR	648	Heat shock protein 70
tr|A0A2I0VX91|A0A2I0VX91_9ASPA	149	Histone H2A
tr|A0A2I0BA63|A0A2I0BA63_9ASPA	134	Histone H2A
tr|A0A2H9ZZ07|A0A2H9ZZ07_9ASPA	155	Histone H2B
tr|A0A5P1EBZ4|A0A5P1EBZ4_ASPOF	157	Histone H2B
tr|A0A2I0A9G7|A0A2I0A9G7_9ASPA	155	Histone H2B.6
tr|A0A2H9ZYM3|A0A2H9ZYM3_9ASPA	103	Histone H4
sp|P78385|KRT83_HUMAN	493	Keratin, type II cuticular Hb3
tr|A0A835S5N5|A0A835S5N5_VANPL	249	l-ascorbate peroxidase
tr|A0A835RYX3|A0A835RYX3_VANPL	293	lactoylglutathione lyase
tr|A0A2I0XCY2|A0A2I0XCY2_9ASPA	663	Luminal-binding protein 4
tr|A0A8T3BYF7|A0A8T3BYF7_DENNO	332	Malate dehydrogenase
sp|P49329|LEC_ALOAR	109	Mannose-specific lectin
tr|A0A5P1FUN5|A0A5P1FUN5_ASPOF	329	Oxygen-evolving enhancer protein 1, chloroplastic
sp|Q40407|PSBP_NARPS	265	Oxygen-evolving enhancer protein 2, chloroplastic
tr|A0A2I0B9H8|A0A2I0B9H8_9ASPA	968	phosphoenolpyruvate carboxylase
tr|A0A2I0AIC2|A0A2I0AIC2_9ASPA	478	Phosphoglycerate kinase
tr|A0A2I0AWP0|A0A2I0AWP0_9ASPA	456	phosphopyruvate hydratase (enolase)
tr|A0A2I0A827|A0A2I0A827_9ASPA	270	Photosystem II 22 kDa protein, chloroplastic
tr|A0A240EY12|A0A240EY12_ALOMC	473	Photosystem II CP43 reaction center protein
tr|A0A7L8ZR22|A0A7L8ZR22_9ASPA	508	Photosystem II CP47 reaction center protein
tr|A0A5P1ET82|A0A5P1ET82_ASPOF	452	Protein kinase domain-containing protein
tr|H2F584|H2F584_ALOVR	477	Ribulose bisphosphate carboxylase large chain
tr|A0A0D4BI40|A0A0D4BI40_9ASPA	348	Ribulose bisphosphate carboxylase large chain (Fragment)
tr|A0A2H9ZVR5|A0A2H9ZVR5_9ASPA	191	Ribulose bisphosphate carboxylase small subunit, chloroplastic
tr|A0A8T3AJS5|A0A8T3AJS5_DENNO	500	RNA polymerase sigma factor sigE, chloroplastic/mitochondrial
tr|A0A5P1FQ00|A0A5P1FQ00_ASPOF	547	RuBisCO large subunit-binding protein subunit alpha
tr|A0A8T3BL71|A0A8T3BL71_DENNO	579	RuBisCO large subunit-binding protein subunit alpha, chloroplastic
sp|P02787|TRFE_HUMAN	698	Serotransferrin
tr|A0A5P1F3D3|A0A5P1F3D3_ASPOF	699	Stromal 70 kDa heat shock-related protein, chloroplastic
tr|A0A5P1E3Q8|A0A5P1E3Q8_ASPOF	273	superoxide dismutase
tr|A0A2I0WUK3|A0A2I0WUK3_9ASPA	269	thioredoxin-dependent peroxiredoxin
tr|A0A5P1FIJ7|A0A5P1FIJ7_ASPOF	442	transaldolase
tr|A0A835V0F1|A0A835V0F1_VANPL	252	Triose-phosphate isomerase
tr|A0A2I0B0Q9|A0A2I0B0Q9_9ASPA	517	Tubulin alpha chain
tr|A0A0K0VH35|A0A0K0VH35_DENOF	447	Tubulin beta chain
tr|A0A2I0A5N1|A0A2I0A5N1_9ASPA	154	Ubiquitin-NEDD8-like protein RUB2
tr|A0A5P1EHB5|A0A5P1EHB5_ASPOF	473	UTP–glucose-1-phosphate uridylyltransferase
tr|A0A2I0BEH3|A0A2I0BEH3_9ASPA	465	UTP–glucose-1-phosphate uridylyltransferase
tr|A0A0A7LU40|A0A0A7LU40_9ASPA	621	V-type proton ATPase catalytic subunit A

(*continued on next page*)

Table 1 (*continued*)

Protein	Length	Protein description
tr|A0A8T3AC29|A0A8T3AC29_DENNO	488	Vacuolar proton pump subunit B
tr|A0A5P1EDP5|A0A5P1EDP5_ASPOF	658	Uncharacterized protein
tr|A0A5P1EV62|A0A5P1EV62_ASPOF	744	Uncharacterized protein
tr|A0A5P1EZQ4|A0A5P1EZQ4_ASPOF	668	Uncharacterized protein
tr|A0A5P1F8R7|A0A5P1F8R7_ASPOF	325	Uncharacterized protein
tr|A0A5P1EBU9|A0A5P1EBU9_ASPOF	617	Uncharacterized protein

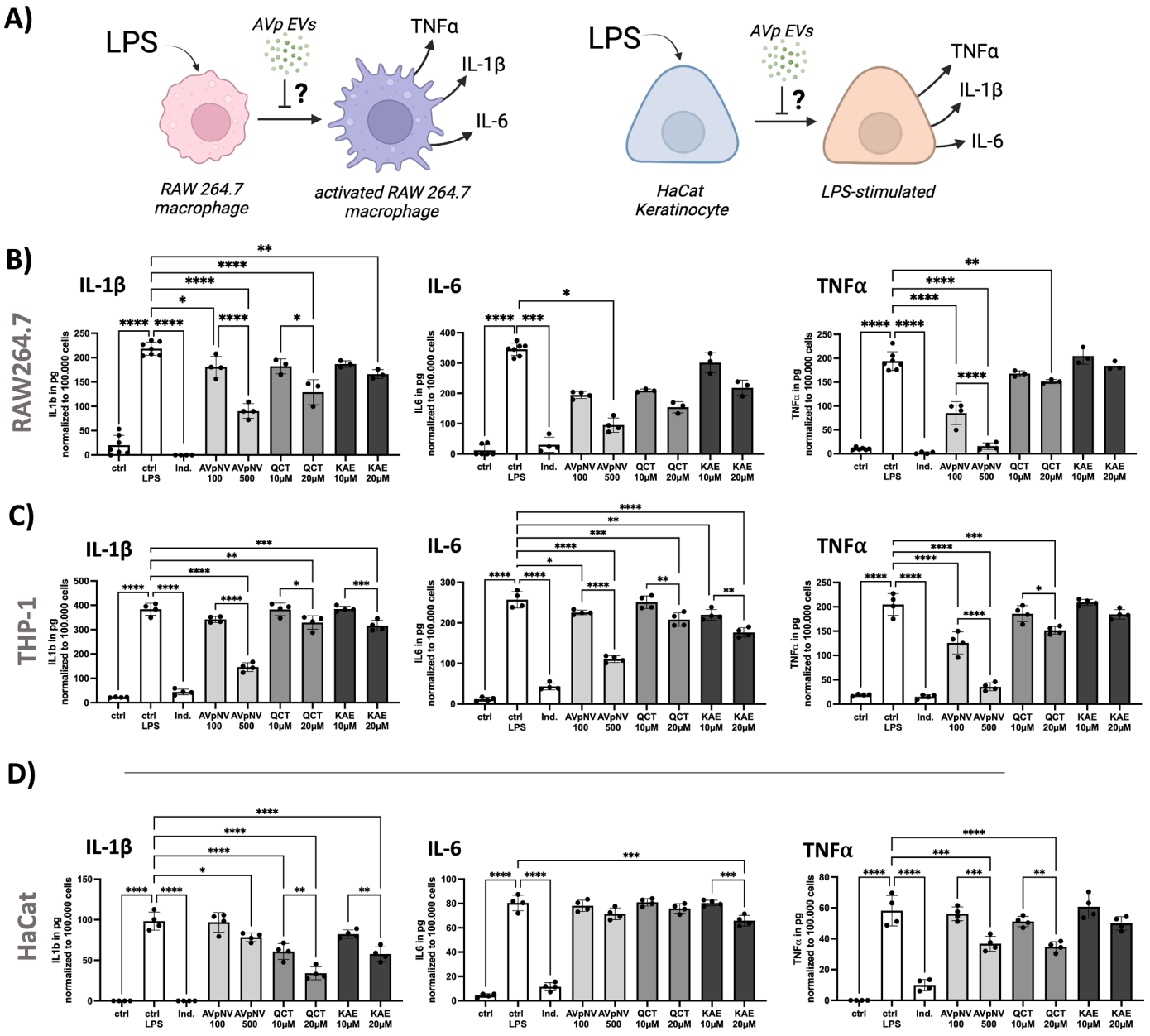

Fig. 3. Effect of AVpNVs on pro-inflammatory cytokine secretion. (A) experimental scheme: RAW264.7 or THP-1 macrophages, as well as HaCat keratinocytes were pre-treated with AVpNVs and stimulated with LPS to induce an inflammatory response. (B/C/D) Cytokines IL-1β, IL-6 and TNFα, secreted by RAW264.7 (B), THP-1 (C), and HaCat (D) cells, were measured with ELISA and normalized on 100.000 cells; Groups ctrl LPS, Indomethacin (Ind.), AVpNV 100, AVpNV 500, QCT 10μM, QCT 20μM, KAE 10μM and KAE 20μM were stimulated with LPS. Data are displayed as mean ± SD, $n = 4$-7. *$p < 0.05$, **$p < 0.01$, ***$p < 0.001$, ****$p < 0.0001$.

(Fig. 1C) and protein concentration was 21.9 ± 12.9 μg/gram of raw material (Fig. 1E). AVpNV size was found to be within the range of 40–200 nm with a mean size of 145 ± 14 nm and a median size of 132 ± 13 nm, respectively (Fig. 1D). To exclude effects based on significant contaminants, total carbohydrate content and the presence of flavonoids were assessed (Fig. 2). In AVp extract, carbohydrates were detected at an average concentration of 1.7 ± 0.7 μg/μl. Quercetin was only detected in one sample (concentration 0.7 μM), while kaempferol was not detected in any samples (Fig. 2A and B). In AVpNVs, neither carbohydrates nor kaempferol or quercetin could be detected (Fig. 2C). However, in AVpNVs an enrichment of total lipids was observed in comparison to AVp extract (117.07 μM compared to 16.8 μM respectively) (Fig. 2D).

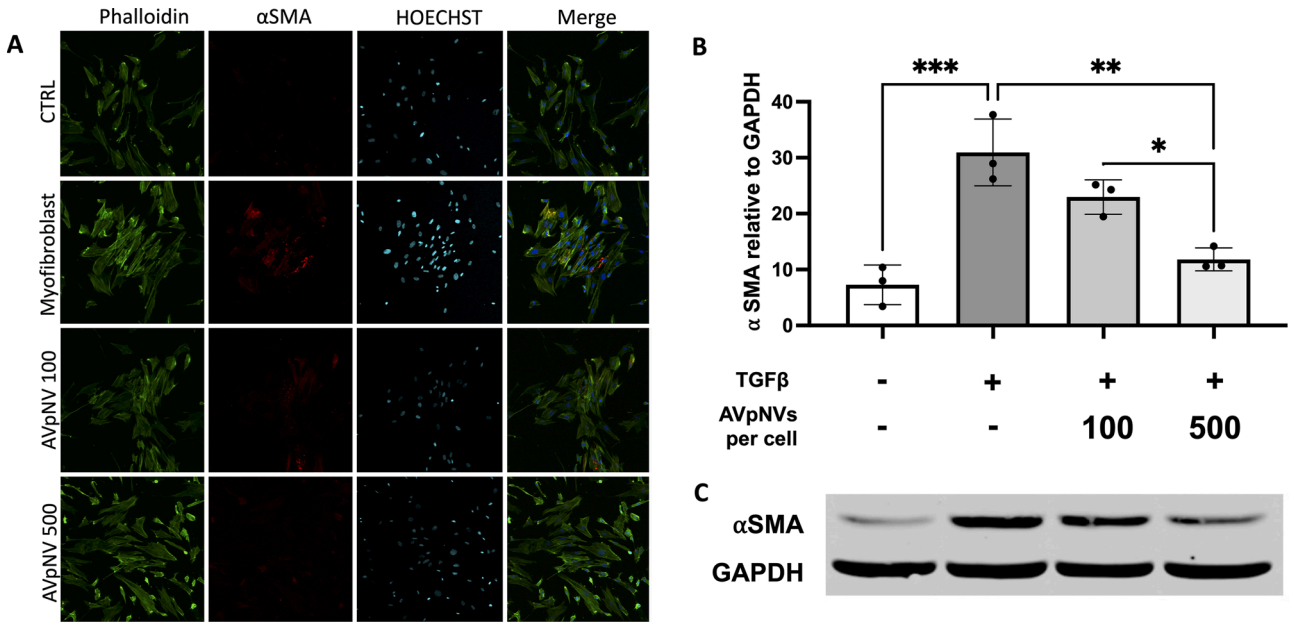

Fig. 4. Effect of AVpNVs on myofibroblast differentiation. (A) Representative confocal microscopy images of HDNF control (CTRL), differentiated myofibroblasts (Myofibroblast), AVpNVs 100/cell (AVpNV 100) and AVpNVs 500/cell (AVpNV 500) stained with Phalloidin (green), α-SMA (red) and HOECHST (blue) 20x magnification; (B/C) Western Blot of HDNF ctrl, differentiated myofibroblasts, AVpNVs 100/cell and AVpNVs 500/cell, stained for α-SMA; (B) α-SMA quantification normalized to GAPDH. Data are displayed as mean ± SD, $n = 3$, $^{*}p < 0.05$, $^{**}p < 0.01$, $^{***}p < 0.001$. (C) Representative Western blot membrane.

With proteomics analysis, it was possible to identify 620 proteins in the AVpNV extract (Supplemental Table 2) and 80 proteins in the AVp-NVs (Table 1). 76 proteins were found in both (Fig. 1F), AVp extract and AVpNVs, while 4 proteins were enriched in AVp-NVs, but could not be detected in AVp extract, namely Glutathione S-transferase P, RNA polymerase sigma factor sigE, Serotransferrin, UTP-glucose-1-phosphate uridylyltransferase.

AVpNVs are cytocompatible and increase keratinocyte proliferation

RAW 264.7 and THP1 M0 macrophages, as well as fibroblasts (HDNF) and keratinocytes (HaCat) were subjected to different concentrations of AVpNVs and flavonoids (kaempferol and quercetin). In all cell types tested, AVpNVs did not exert a decrease in metabolic activity (MTT assay), or an increase in cell damage (LDH assay) (Supplemental Figs. 1, 2). Interestingly, the higher concentrations of flavonoids did decrease metabolic activity in RAW264.7, HDNF and HaCat cells after 24 h. However, no increase in cell damage was observed. 500 AVpNVs per cell led to a 9.8% increase in proliferation of keratinocytes, while no effects on fibroblast proliferation were observed. (Supplemental Fig. 1).

AVpNVs reduce the secretion of pro-inflammatory cytokines in burn-wound-associated cells

To assess the anti-inflammatory potential of AVpNVs, RAW264.7 and THP-1 M0 macrophages, as well as HaCat cells were pre-treated with 2 ratios of AVpNVs, (100/ 500 NVs per cell), and subsequently exposed to LPS (Fig. 3A). LPS significantly increased the secretion of IL-1β, IL-6 and TNFα in all the tested cell types, while indomethacin inhibited secretion to baseline level. Exact mean values +/- SD are available in Supplemental Table 1.

For murine RAW 264.7 macrophages, AVpNVs 500/cell led to a significant reduction of all three tested cytokines, while the lower concentration AVpNVs 100/cell significantly reduced IL-1β and TNFα. The lower concentrations of quercetin and kaempferol (10 μM) did not display effects, but 20 μM kaempferol significantly reduced secretion of IL-1β, and 20 μM quercetin IL-1β and TNFα. In both cases the effect was less pronounced than for AVpNVs 500/cell. (Fig. 3B)

Human THP-1 cells displayed a significant reduction of IL-6, TNFα, but not IL-1β, in presence of the low AVpNV concentration (100/cell). Secretion of all three cytokines was significantly reduced when exposed to the high AVpNV concentration (500/cell) and quercetin 20 μM. Kaempferol 10 μM reduced secretion of IL-6 to a comparable level as AVpNV 100/cell and quercetin 20 μM, and the higher concentration (20 μM) led to a significant reduction of IL-1β and IL-6. Secretion of TNFα was unaffected by kaempferol in THP-1 cells (Fig. 3C).

In the human keratinocyte cell line HaCat, the low concentration of AVpNVs (100/cell) did not reduce secretion of pro-inflammatory cytokines, while the higher concentration (500/cell) lead significantly reduced IL-1β and TNFα. AVpNVs had no effect on the secretion of IL-6 in HaCat cells. Quercetin 10 μM significantly reduced IL-1β, while the higher concentration 20 μM also displayed effects on TNFα, but not on IL-6. Kaempferol 20 μM on the other hand decreased the secretion of IL-1β and IL6, but not TNFα (Fig. 3D).

AVpNVs diminish TGF-β mediated myofibroblast differentiation

Myofibroblast differentiation was induced in HDNF cultures exposed to TGFβ1, simultaneously in the presence of AVpNVs Fig. 4A demonstrates actin filaments and formed stressed fibers accumulating αSMA in the myofibroblast group. The undifferentiated control group as well as the AVpNV 500 group did not stain positive for αSMA. Furthermore, αSMA was quantified by western blot as a differentiation marker of myofibroblasts (Fig. 4B). TGFβ1 induced a 5-time increase in the αSMA signal compared to HDNF without TGFβ1 (normalized to GAPDH). However, AVpNVs treatment reduced αSMA signal by 24.4 ± 14.8% and 60.3 ± 13.1% with a ratio of 100 and 500 particles per cell, respectively, compared to the TGF-β-induced control (Fig. 4B and C).

AVpNVs reduce cellular contraction in fibroblasts and myofibroblasts

Contractile capacity of HDNF and myofibroblasts was assessed within type-1 collagen hydrogels by measuring the gel area after 24 h incubation. Untreated myofibroblasts contracted collagen gels significantly more than HDNF cells (57.9% ± 6.5% and 47.4% ± 3.2% contraction, respectively). LPA significantly stimulated contraction in

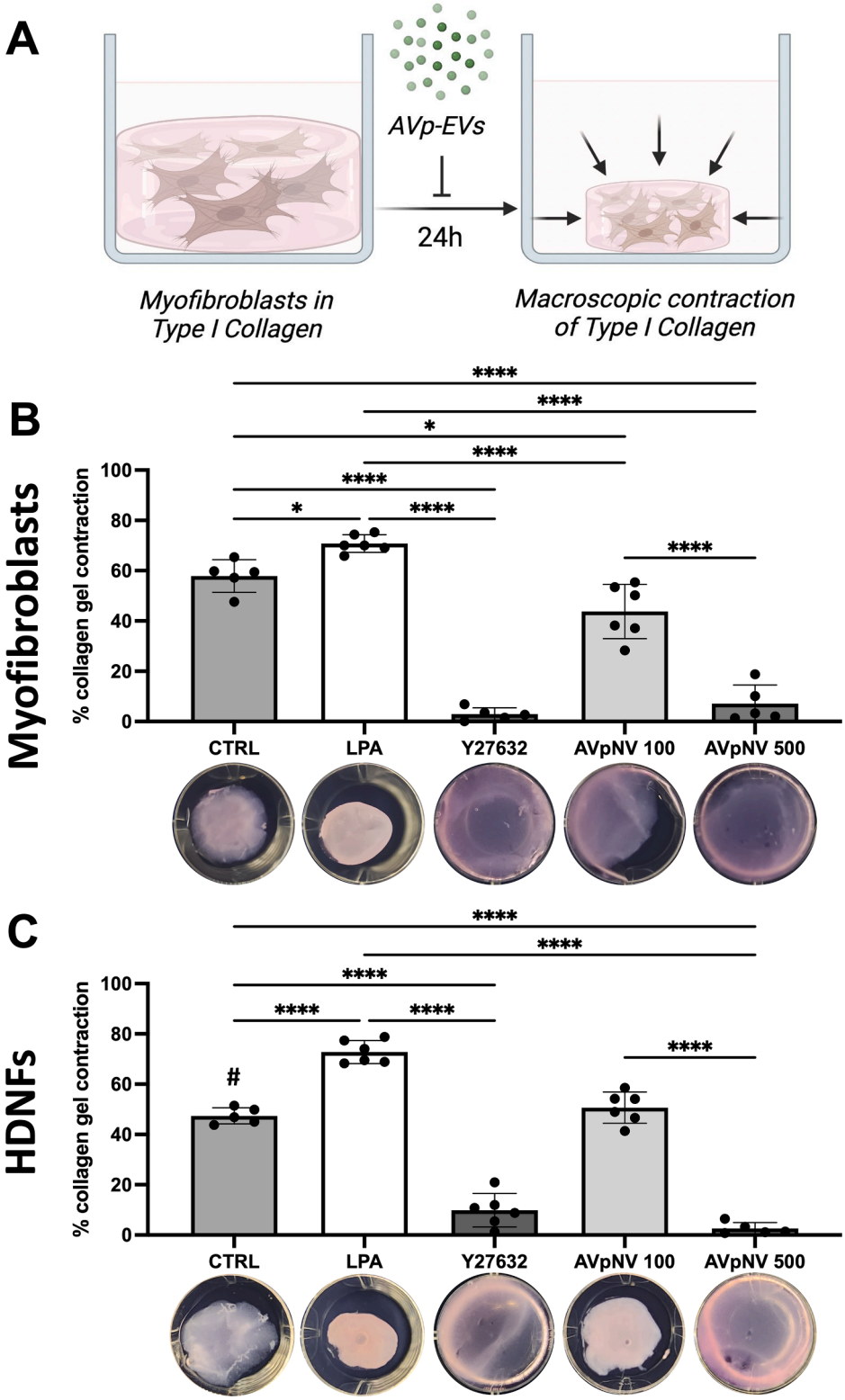

Fig. 5. Effect of AVpNVs on cellular contraction. (A) experimental scheme: HDNF and myofibroblasts were seeded in type I collagen matrices in the presence and absence of AVpNVs, and the area covered by collagen was measured after 24 h. (B/C) Quantification of collagen gel contraction compared to timepoint zero of untreated gels, and representative images of collagen gels at time point 24 h. Groups tested were untreated control (CTRL), LPA (positive control), inhibitor Y27632 (negative control) as well as gels containing 100 and 500 AVpNVs per cell (AVpNV); Cells tested were (B) myofibroblast and (C) HDNF cells. data displayed as mean ± SD, $n = 6$, $^{*}p < 0.05$, $^{**}p < 0.01$, $^{***}p < 0.001$, $^{****}p < 0.0001$.

both, HNDFs (72.8% ± 4.6%) and myofibroblasts (70.81 ± 3.5%), while Y27632 inhibited contraction (9.9% ± 6.7% and 3.0 % ± 2.5%, respectively). AVpNVs 500/cell reduced contractability in both cell types compared to unstimulated control and LPA-stimulated control (Myofibroblasts 2.6% ± 2.4%., HDNF 7.1 % ± 6.9%). In myofibroblasts, AVpNVs 100/cell also had a significant effect on contraction (43.8% ± 10.8%) (Fig. 5B/C).

Discussion

Plant-based industries produce large amounts of by-products that are considered waste material, and as a consequence, the exploration of new strategies to utilize these resources looks to contribute to a more sustainable economy. In this study, we confirmed the findings by Kim et al. (2021) that *Aloe vera* peels contain NVs, however, using passive diffusion instead of blending for pre-isolation. In contrast to blending, passive diffusion reduces the isolation of contaminants, such as carbohydrates and flavonoids, which have shown effects in the past (Balan et al., 2014; Vázquez et al., 1996). We analyzed AVpNVs and pre-isolation AVp extracts regarding the presence of carbohydrates, kaempferol and quercetin, in order to exclude that the effects found in this study are due to co-isolated compounds. We could only detect carbohydrates in the pre-isolation AVp extracts, and quercetin in one of the AVp extracts (Fig. 2B, C). Since *Aloe vera* usually contains both flavonoids, we hypothesize that their absence is based on their low solubility in water and PBS at room temperature (PubChem: Kaempferol 0.44 mg/ml; Quercetin: 0.06 mg/ml). On the other hand, we could demonstrate an enrichment of lipids in AVpNVs (Fig. 2D), which strengthens the assumption that vesicles are present in the isolate. This was confirmed by TEM and AFM (Fig. 1A, B). Interestingly, AFM visualization in atmospheric conditions, displays round, spherical vesicles and not the cup-shaped morphology. A similar morphology was observed by our group in previous studies using AFM for visualization of non-mammalian EVs (Álvarez et al., 2023; Leiva-Sabadini et al., 2021). NTA analysis revealed no significant difference between average (mean) and median size, indicating no significant secondary population in the isolates. Proteomic analysis found proteins associated with plant vesicles in the AVpNV isolate, including HSP70, Histone H4 and actin (Deng and Miller, 2019; Nemati et al., 2022; Ortiz, 2017) while known negative EV/NV markers such as Calnexin and Cytochrome C (ISEV) were only present in AVp extract. In recent yr a number of new proteins associated with EV enrichment have been described, including protein 14-3-3 and enolase (Wang, Li Qun), which have also been detected in AVpNVs. Summarizing, AVpNV contain highly-purified NVs in the absence of other relevant biologically-active compounds, and display an enrichment of several noteworthy markers associated with EVs/NVs.

AVpNVs have demonstrated to be biocompatible with important skin cells such as dermal fibroblasts and keratinocytes. Furthermore, they display important therapeutical properties such as radical scavenging and stimulation of cell migration that might favor the treatment of pathologies like chronic wounds (Kim et al., 2021). In the present study, we have also confirmed AVpNV biocompatibility in human dermal fibroblasts and two macrophage cell lines (Supplemental Figs. 1 and 2). Inflammation intensity in the acute phase of wound healing correlates with the final scar size, and the modulation of this process is currently considered a key target for scar management (Wang et al., 2020). The use of phenolic compounds in wound healing is hampered by their low solubility and poor skin penetration, thus, lipid nanoparticles and microemulsions have been assessed as potential alternatives (Butkeviciute et al., 2022; Oliveira et al., 2022). Within this context, vesicles are gaining attention as drug carriers because of their storage stability, cargo protection, and small size which is suitable for different treatment strategies (Cheng and Hill, 2022).

Furthermore, our results demonstrate that AVpNVs reduce the secretion of pro-inflammatory cytokines (Fig. 3), in both, human and murine macrophages as well as HaCat keratinocytes. Until today, these known anti-inflammatory effects of *Aloe vera* have been mostly attributed to phenolic compounds such as quercetin and kaempferol (Domínguez-Avila et al., 2022; Xia et al., 2021). As mentioned above, both flavonoids could not be detected in AVpNV samples. Furthermore, AVpNVs displayed an overall more pronounced anti-inflammatory effect in macrophages: while kaempferol and quercetin decreased pro-inflammatory cytokines in the range of 10–53% in high concentrations (20 μM), AVpNVs decreased secretion between 59 and 91 % (Fig. 3). These results found for quercetin and kaempferol are consistent with the previous assessments found in literature (Endale et al., 2013; Khajuria et al., 2018). Interestingly, no effect of AVpNVs on Il-6 was observed in keratinocytes, however, kaempferol 20 μM did decrease by 18.1%. Wu et al. discovered that IL-6 secretion was modulated by the microRNA Let-7, which has not been found in *Aloe vera*. Altogether, our results suggest that the anti-inflammatory effect displayed by AVpNVs is not mediated by the presence of phenolic compounds, and that the resulting modulation of pro-inflammatory cytokines is actually increased in AVpNVs when compared to kaempferol and quercetin. Proteomic analysis revealed the presence of anti-inflammatory proteins, such as phosphoenolpyruvate carboxy kinase (Pck1) and Glutathione S-transferase P (GSTP1) in AVpNVs. Especially the latter, GSTP1, is of interest, since it was among the proteins that were not detected in AVp extract. A recent study of Russel et al. revealed a novel role of GSTP1: overexpression in macrophages decreased the acute inflammatory response in an LPS-stimulated *in vivo* mouse model (Russell and Richardson, 2023). Pck1 has demonstrated regulatory roles: deletion of Pck1 lead to higher inflammatory responses in macrophages (Ko et al., 2018). Furthermore, Kim et al. (2021) found a strong anti-oxidant role of AVpNVs, however, did not study active components present in AVpNVs. Peroxiredoxins, such as thioredoxin-dependent peroxiredoxin present in AVpNVs have been found to be effective against oxidative stress, which again plays a crucial role in inflammation (Zhang et al., 2020).

On the other hand, dermal fibroblasts and myofibroblasts are responsible for dermis regeneration and remodeling. A strong inflammatory response in the acute phase is linked to aberrant fibroblast recruitment that leads to scar formation (Mack, 2018). TGFβ1 secreted by fibroblasts and immune cells triggers myofibroblast differentiation of dermal fibroblasts embedded in the granulation tissue (Desmoulière et al., 1993; Pakshir et al., 2020; Penn et al., 2012). Under normal circumstances, the presence of myofibroblasts favors wound healing due to collagen deposition in the proliferative phase and contractile forces that accelerate the closure of wound borders. When myofibroblasts undergo apoptosis, callous remodeling is started by adjacent fibroblasts (Nedelec et al., 2001; Sorg et al., 2017). However, myofibroblasts are persistent in hypertrophic scars, and are associated with a chronic state of inflammation within the fibrotic tissue (Nedelec et al., 2001; Ogawa, 2017). In this context, TGFβ1 signaling and myofibroblasts have become key targets in scar therapy. Our results show that AVpNVs reduce myofibroblast differentiation of dermal fibroblasts (Fig. 4) as well as their collagen contractile capacity (Fig. 5). In our model, kaempferol and quercetin did not affect myofibroblast differentiation (Supplemental Fig. 3). Proteomic analysis revealed an enrichment of superoxide dismutase in AVpNVs, which has been demonstrated to be anti-fibrotic, leading to a reversion of the myofibroblast phenotype (Vozenin--Brotons et al., 2001).

Current strategies in burn wounds are based on corticosteroid injections, which require close medical vigilance since local immune suppression might lead to uncontrolled bacterial colonization (Altarrah et al., 2022; Fuchs et al., 2007). Use of nonsteroidal anti-inflammatory drugs (NSAID) have a short term relieve of inflammation and pain that might reduce hypertrophic scars (Rahmani-Neishaboor et al., 2010; Wang et al., 2020) but with the risk of developing adverse drug reaction and delaying wound healing due to suppression of prostaglandin 2 (Gallelli et al., 2007).

Novel strategies for burn wound treatment seek to decrease scarring on a cellular and molecular level in early stages of wound healing. In this

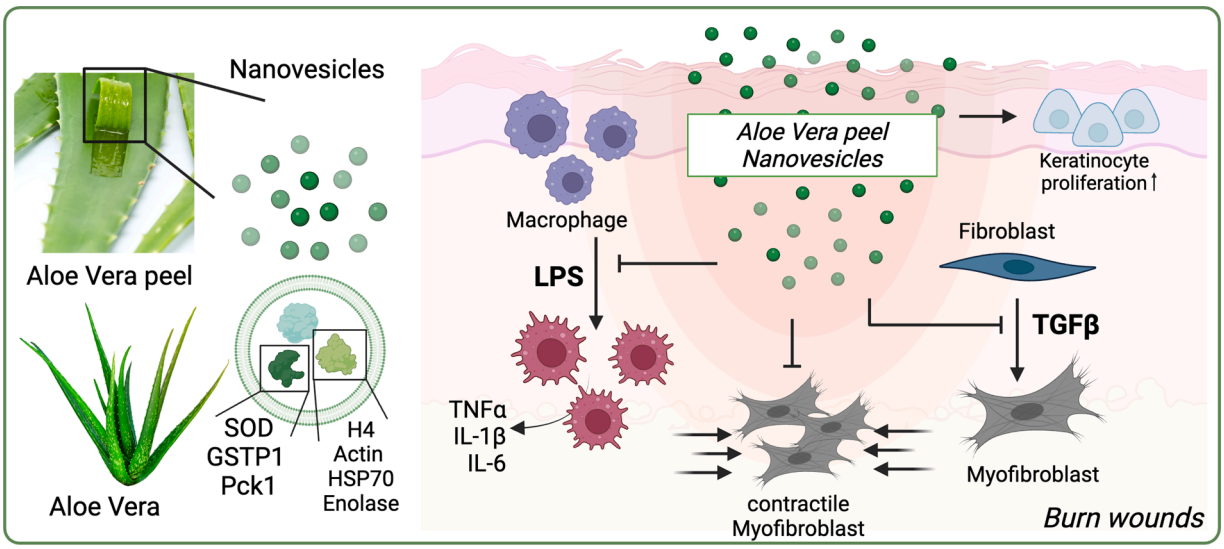

Fig. 6. Graphical summary; Nanovesicles were confirmed to be present in *Aloe vera* peel (AVpNVs). Proteomic analysis revealed the presence of vesicle-associated proteins such as H4, actin, enolase or HSP70, as well as active components such as SOD, GSTP1 and Pck1. AVpNVs displayed anti-inflammatory effects, promoted keratinocyte proliferation and inhibited myofibroblast differentiation and contraction.

study, we performed an analysis of isolated AVpNVs, confirming a homogenous NV population, the absence of flavonoid or carbohydrate contaminants, and the presence of lipids as well as proteins associated to EVs/NVs. We report anti-inflammatory properties of AVpNVs in different cell types from different species, confirming a strong anti-inflammatory effect in mouse and human macrophages, as well as human keratinocytes. Furthermore, we discovered that AVpNVs inhibit TGFβ-stimulated myofibroblast differentiation and diminish the contractile properties of both, fibroblasts and myofibroblasts *in vitro*. Finally, we were the first to assess the protein profile of AVpNVs in comparison to AVp extract, and were able to link the observed effects to proteins present in AVpNVs (summarized in Fig. 6). Further studies are needed to assess appropriate biomaterials for the topical release of AVpNVs into the wound bed, and, subsequently, *in vivo* studies confirming the effects in a pre-clinical model.

CRediT authorship contribution statement

Orlando Ramírez: Data curation, Formal analysis, Writing – original draft, Writing – review & editing. **Florencia Pomareda:** Data curation, Formal analysis, Writing – review & editing. **Belén Olivares:** Data curation, Formal analysis, Writing – review & editing. **Ya-Lin Huang:** Data curation, Formal analysis, Writing – review & editing. **Gabriela Zavala:** Data curation, Formal analysis, Writing – review & editing, Visualization. **Javiera Carrasco-Rojas:** Data curation, Formal analysis, Writing – review & editing. **Simón Álvarez:** Data curation, Formal analysis, Writing – review & editing, Visualization. **Camila Leiva-Sabadini:** Data curation, Formal analysis, Writing – review & editing. **Valeria Hidalgo:** Data curation, Formal analysis, Writing – review & editing. **Pablo Romo:** Data curation, Formal analysis, Writing – review & editing. **Matías Sánchez:** Data curation, Formal analysis, Writing – review & editing. **Ayleen Vargas:** Data curation, Formal analysis, Writing – review & editing. **Jessica Martínez:** Data curation, Formal analysis, Supervision, Writing – review & editing. **Sebastian Aguayo:** Data curation, Formal analysis, Supervision, Visualization, Writing – review & editing. **Christina M.A.P. Schuh:** Conceptualization, Funding acquisition, Data curation, Formal analysis, Visualization, Supervision, Writing – original draft, Writing – review & editing.

Declaration of Competing Interest

The authors report no conflict of interest.

Acknowledgments

This work was financially supported by the independent funding agency ANID Chile (Agencia Nacional de Investigación y Desarrollo), under the grant scheme FONDECYT regular (#1220803 and #1220804). Authors would like to thank the Advanced Microscopy Unit (UMA UC) for their support with the TEM. Furthermore, authors acknowledge the MELISA Institute (San Pedro de la Paz, Chile) for providing the infrastructure and human resources to perform proteomics analysis. Figs. 3A, 5A and 6 were created with BioRender.com, license for publication was purchased by CS.

Supplementary materials

Supplementary material associated with this article can be found, in the online version, at doi:10.1016/j.phymed.2023.155108.

References

Agrahari, Vivek, Agrahari, V., Burnouf, P.A., Chew, C.H., Burnouf, T., 2019. Extracellular microvesicles as new industrial therapeutic frontiers. Trends Biotechnol. 37, 707–729. https://doi.org/10.1016/j.tibtech.2018.11.012.

Altarrah, K., Tan, P., Acharjee, A., Hazeldine, J., Torlinska, B., Wilson, Y., Torlinski, T., Moiemen, N., Lord, J.M., 2022. Differential benefits of steroid therapies in adults following major burn injury. J. Plast. Reconstr. Aesthetic Surg. 75, 2616–2624. https://doi.org/10.1016/j.bjps.2022.04.007.

Álvarez, S., Contreras-Kallens, P., Aguayo, S., Ramírez, O., Vallejos, C., Ruiz, J., Carrasco-Gallardo, E., Troncoso-Vera, S., Morales, B., Schuh, C.M.A.P., 2023. Royal jelly extracellular vesicles promote wound healing by modulating underlying cellular responses. Mol. Ther. Nucleic Acids 31, 541–552. https://doi.org/10.1016/j.omtn.2023.02.008.

Balan, B.J., Niemcewicz, M., Kocik, J., Jung, L., Skopińska-Różewska, E., Skopiński, P., 2014. Experimental immunologyOral administration of *Aloe vera* gel, anti-microbial and anti-inflammatory herbal remedy, stimulates cell-mediated immunity and antibody production in a mouse model. Cent. Eur. J. Immunol. 39, 125–130. https://doi.org/10.5114/ceji.2014.43711.

Bijlard, E., Uiterwaal, L., Kouwenberg, C.A., Mureau, M.A., Hovius, S.E., Huygen, F.J., 2017. A systematic review on the prevalence, etiology, and pathophysiology of intrinsic pain in dermal scar tissue. Pain Physician 20, 1–13.

Bombaro, K.M., Engrav, L.H., Carrougher, G.J., Wiechman, S.A., Faucher, L., Costa, B.A., Heimbach, D.M., Rivara, F.P., Honari, S., 2003. What is the prevalence of hypertrophic scarring following burns? Burns 29, 299–302. https://doi.org/10.1016/S0305-4179(03)00067-6.

Burusapat, C., Supawan, M., Pruksapong, C., Pitiseree, A., Suwantemee, C., 2018. Topical *Aloe vera* gel for accelerated wound healing of split-thickness skin graft donor sites: a double-blind, randomized, controlled trial and systematic review. Plast. Reconstr. Surg. 142, 217–226.

Butkeviciute, A., Ramanauskiene, K., Kurapkiene, V., Janulis, V., 2022. Dermal penetration studies of potential phenolic compounds *ex vivo* and their antioxidant activity *in vitro*. Plants. https://doi.org/10.3390/plants11151901.

Cheng, L., Hill, A.F., 2022. Therapeutically harnessing extracellular vesicles. Nat. Rev. Drug Discov. 21, 379–399. https://doi.org/10.1038/s41573-022-00410-w.

Colombo, M., Melchiades, G., de, L., Figueiró, F., Battastini, A.M.O., Teixeira, H.F., Koester, L.S., 2017. Validation of an HPLC-UV method for analysis of Kaempferol-loaded nanoemulsion and its application to *in vitro* and *in vivo* tests. J. Pharm. Biomed. Anal. 145, 831–837. https://doi.org/10.1016/j.jpba.2017.07.046.

Deng, F., Miller, J., 2019. A review on protein markers of exosome from different bio-resources and the antibodies used for characterization. J. Histotechnol. 42, 226–239. https://doi.org/10.1080/01478885.2019.1646984.

Desmoulière, A., Geinoz, A., Gabbiani, F., Gabbiani, G., 1993. Transforming growth factor-beta 1 induces alpha-smooth muscle actin expression in granulation tissue myofibroblasts and in quiescent and growing cultured fibroblasts. J. Cell Biol. 122, 103–111. https://doi.org/10.1083/jcb.122.1.103.

Domínguez-Avila, J.A., Salazar-López, N.J., Montiel-Herrera, M., Martínez-Martínez, A., Villegas-Ochoa, M.A., González-Aguilar, G.A., 2022. Phenolic compounds can induce systemic and central immunomodulation, which result in a neuroprotective effect. J. Food Biochem. 46, e14260. https://doi.org/10.1111/jfbc.14260.

Endale, M., Park, S.C., Kim, S., Kim, S.H., Yang, Y., Cho, J.Y., Rhee, M.H., 2013. Quercetin disrupts tyrosine-phosphorylated phosphatidylinositol 3-kinase and myeloid differentiation factor-88 association, and inhibits MAPK/AP-1 and IKK/NF-κB-induced inflammatory mediators production in RAW 264.7 cells. Immunobiology 218, 1452–1467. https://doi.org/10.1016/j.imbio.2013.04.019.

Fuchs, P.C., Bozkurt, A., Johnen, D., Smeets, R., Groger, A., Pallua, N., 2007. Beneficial effect of corticosteroids in catecholamine-dependent septic burn patients. Burns 33, 306–311. https://doi.org/10.1016/j.burns.2006.07.026.

Gallelli, L., Colosimo, M., Pirritano, D., Ferraro, M., De Fazio, S., Marigliano, N.M., De Sarro, G., 2007. Retrospective evaluation of adverse drug reactions induced by nonsteroidal anti-inflammatory drugs. Clin. Drug Investig. 27, 115–122. https://doi.org/10.2165/00044011-200727020-00004.

Gao, C., Zhou, Y., Chen, Z., Li, H., Xiao, Y., Hao, W., Zhu, Y., Vong, C.T., Farag, M.A., Wang, Y., Wang, S., 2022. Turmeric-derived nanovesicles as novel nanobiologics for targeted therapy of ulcerative colitis. Theranostics 12, 5596–5614. https://doi.org/10.7150/thno.73650.

Hade, M.D., Suire, C.N., Mossell, J., Suo, Z., 2022. Extracellular vesicles: emerging frontiers in wound healing. Med. Res. Rev. 42, 2102–2125. https://doi.org/10.1002/med.21918.

James, S.L., Lucchesi, L.R., Bisignano, C., Castle, C.D., Dingels, Z.V., Fox, J.T., Hamilton, E.B., Henry, N.J., McCracken, D., Roberts, N.L.S., Sylte, D.O., Ahmadi, A., Ahmed, M.B., Alahdab, F., Alipour, V., Andualem, Z., Antonio, C.A.T., Arabloo, J., Badiye, A.D., Bagherzadeh, M., Banstola, A., Bärnighausen, T.W., Barzegar, A., Bayati, M., Bhaumik, S., Bijani, A., Bukhman, G., Carvalho, F., Crowe, C.S., Dalal, K., Daryani, A., Nasab, M.D., Do, H.T., Do, H.P., Endries, A.Y., Fernandes, E., Filip, I., Fischer, F., Fukumoto, T., Gebremedhin, K.B.B., Gebremeskel, G.G., Gilani, S.A., Haagsma, J.A., Hamidi, S., Hostiuc, S., Househ, M., Igumbor, E.U., Ilesanmi, O.S., Irvani, S.S.N., Jayatilleke, A.U., Kahsay, A., Kapoor, N., Kasaeian, A., Khader, Y.S., Khalil, I.A., Khan, E.A., Khazaee-Pool, M., Kokubo, Y., Lopez, A.D., Madadin, M., Majdan, M., Maled, V., Malekzadeh, R., Manafi, N., Manafi, A., Mangalam, S., Massenburg, B.B., Meles, H.G., Menezes, R.G., Meretoja, T.J., Miazgowski, B., Miller, T.R., Mohammadian-Hafshejani, A., Mohammadpourhodki, R., Morrison, S. D., Negoi, I., Nguyen, T.H., Nguyen, S.H., Nguyen, C.T., Nixon, M.R., Olagunju, A.T., Olagunju, T.O., Padubidri, J.R., Polinder, S., Rabiee, N., Rabiee, M., Radfar, A., Rahimi-Movaghar, V., Rawaf, S., Rawaf, D.L., Rezapour, A., Rickard, J., Roro, E.M., Roy, N., Safari-Faramani, R., Salamati, P., Samy, A.M., Satpathy, M., Sawhney, M., Schwebel, D.C., Senthilkumaran, S., Sepanlou, S.G., Shigematsu, M., Soheili, A., Stokes, M.A., Tohidinik, H.R., Tran, B.X., Valdez, P.R., Wijeratne, T., Yisma, E., Zaidi, Z., Zamani, M., Zhang, Z.J., Hay, S.I., Mokdad, A.H., 2020. Epidemiology of injuries from fire, heat and hot substances: global, regional and national morbidity and mortality estimates from the Global Burden of Disease 2017 study. Inj. Prev. 26 https://doi.org/10.1136/injuryprev-2019-043299 i36 LP-i45.

Khajuria, V., Gupta, S., Sharma, N., Tiwari, H., Bhardwaj, S., Dutt, P., Satti, N., Nargotra, A., Bhagat, A., Ahmed, Z., 2018. Kaempferol-3-o-β-d-glucuronate exhibit potential anti-inflammatory effect in LPS stimulated RAW 264.7 cells and mice model. Int. Immunopharmacol. 57, 62–71. https://doi.org/10.1016/j.intimp.2018.01.041.

Kim, M., Park, J.H., 2022. Isolation of aloe saponaria-derived extracellular vesicles and investigation of their potential for chronic wound healing. Pharmaceutics. https://doi.org/10.3390/pharmaceutics14091905.

Kim, M.K., Choi, Y.C., Cho, S.H., Choi, J.S., Cho, Y.W., 2021. The antioxidant effect of small extracellular vesicles derived from *Aloe vera* peels for wound healing. Tissue Eng. Regen. Med. 18, 561–571. https://doi.org/10.1007/s13770-021-00367-8.

Ko, C.W., Counihan, D., Wu, J., Hatzoglou, M., Puchowicz, M.A., Croniger, C.M., 2018. Macrophages with a deletion of the phosphoenolpyruvate carboxykinase 1(Pck1) gene have a more proinflammatory phenotype. J. Biol. Chem. 293, 3399–3409. https://doi.org/10.1074/jbc.M117.819136.

Leiva-Sabadini, C., Alvarez, S., Barrera, N.P., Schuh, C.M.A.P., Aguayo, S., 2021. Antibacterial effect of honey-derived exosomes containing antimicrobial peptides against oral streptococci. Int. J. Nanomed. 16, 4891–4900. https://doi.org/10.2147/IJN.S315040.

Mack, M., 2018. Inflammation and fibrosis. Matrix Biol. 68-69, 106–121. https://doi.org/10.1016/j.matbio.2017.11.010.

Maenthaisong, R., Chaiyakunapruk, N., Niruntraporn, S., Kongkaew, C., 2007. The efficacy of *Aloe vera* used for burn wound healing: a systematic review. Burns 33, 713–718. https://doi.org/10.1016/j.burns.2006.10.384.

Moulin, V., Larochelle, S., Langlois, C., Thibault, I., Lopez-Vallé, C.A., Roy, M., 2004. Normal skin wound and hypertrophic scar myofibroblasts have differential responses to apoptotic inductors. J. Cell. Physiol. https://doi.org/10.1002/jcp.10415.

Nedelec, B., Shankowsky, H., Scott, P.G., Ghahary, A., Tredget, E.E., 2001. Myofibroblasts and apoptosis in human hypertrophic scars: the effect of interferon-α2b. Surgery 130, 798–808.

Nemati, Mohadeseh, Singh, B., Mir, R.A., Nemati, Mahdieh, Babaei, A., Ahmadi, M., Rasmi, Y., Golezani, A.G., Rezaie, J., 2022. Plant-derived extracellular vesicles: a novel nanomedicine approach with advantages and challenges. Cell Commun. Signal. 20, 69. https://doi.org/10.1186/s12964-022-00889-1.

Ogawa, R., 2017. Keloid and hypertrophic scars are the result of chronic inflammation in the reticular dermis. Int. J. Mol. Sci. https://doi.org/10.3390/ijms18030606.

Oliveira, A.L.S., Valente, D., Moreira, H.R., Pintado, M., Costa, P., 2022. Effect of squalane-based emulsion on polyphenols skin penetration: *ex vivo* skin study. Colloids Surf. B Biointerfaces 218, 112779. https://doi.org/10.1016/j.colsurfb.2022.112779.

Ortiz, A., 2017. Not all extracellular vesicles were created equal: clinical implications. Ann. Transl. Med. 5. No 5 (March 15, 2017) Ann. Transl. Med.

Pakshir, P., Noskovicova, N., Lodyga, M., Son, D.O., Schuster, R., Goodwin, A., Karvonen, H., Hinz, B., 2020. The myofibroblast at a glance. J. Cell Sci. 133 https://doi.org/10.1242/jcs.227900 jcs227900.

Penn, J.W., Grobbelaar, A.O., Rolfe, K.J., 2012. The role of the TGF-β family in wound healing, burns and scarring: a review. Int. J. Burn. Trauma 2, 18–28.

Rahmani-Neishaboor, E., Yau, F.M., Jalili, R., Kilani, R.T., Ghahary, A., 2010. Improvement of hypertrophic scarring by using topical anti-fibrogenic/anti-inflammatory factors in a rabbit ear model. Wound Repair Regen. 18, 401–408. https://doi.org/10.1111/j.1524-475X.2010.00598.x.

Raimondo, S., Naselli, F., Fontana, S., Monteleone, F., Lo Dico, A., Saieva, L., Zito, G., Flugy, A., Manno, M., Di Bella, M.A., De Leo, G., Alessandro, R., 2015. Citrus limon-derived nanovesicles inhibit cancer cell proliferation and suppress CML xenograft growth by inducing TRAIL-mediated cell death. Oncotarget 6, 19514–19527. https://doi.org/10.18632/oncotarget.4004.

Raimondo, S., Urzì, O., Meraviglia, S., Di Simone, M., Corsale, A.M., Rabienezhad Ganji, N., Palumbo Piccionello, A., Polito, G., Lo Presti, E., Dieli, F., Conigliaro, A., Alessandro, R., 2022. Anti-inflammatory properties of lemon-derived extracellular vesicles are achieved through the inhibition of ERK/NF-κB signalling pathways. J. Cell. Mol. Med. 26, 4195–4209. https://doi.org/10.1111/jcmm.17404.

Russell, T.M., Richardson, D.R., 2023. The good Samaritan glutathione-S-transferase P1: an evolving relationship in nitric oxide metabolism mediated by the direct interactions between multiple effector molecules. Redox Biol. 59, 102568 https://doi.org/10.1016/j.redox.2022.102568.

Sánchez, J.L.A., Perepérez, S.B., Bastida, J.L., Martínez, M.M., 2007. Cost-utility analysis applied to the treatment of burn patients in a specialized center. Arch. Surg. https://doi.org/10.1001/archsurg.142.1.50.

Schuh, C.M.A.P., Aguayo, S., Zavala, G., Khoury, M., 2019. Exosome-like vesicles in Apis mellifera bee pollen, honey and royal jelly contribute to their antibacterial and pro-regenerative activity. J. Exp. Biol. 222 https://doi.org/10.1242/jeb.208702.

Slemp, A.E., Kirschner, R.E., 2006. Keloids and scars: a review of keloids and scars, their pathogenesis, risk factors, and management. Curr. Opin. Pediatr. https://doi.org/10.1097/01.mop.0000236389.41462.ef.

Sorg, H., Tilkorn, D.J., Hager, S., Hauser, J., Mirastschijski, U., 2017. Skin wound healing: an update on the current knowledge and concepts. Eur. Surg. Res. 58, 81–94. https://doi.org/10.1159/000454919.

Vázquez, B., Avila, G., Segura, D., Escalante, B., 1996. Antiinflammatory activity of extracts from *Aloe vera* gel. J. Ethnopharmacol. 55, 69–75. https://doi.org/10.1016/S0378-8741(96)01476-6.

Vozenin-Brotons, M.C., Sivan, V., Gault, N., Renard, C., Geffrotin, C., Delanian, S., Lefaix, J.L., Martin, M., 2001. Antifibrotic action of Cu/Zn SOD is mediated by TGF-β1 repression and phenotypic reversion of myofibroblasts. Free Radic. Biol. Med. 30, 30–42. https://doi.org/10.1016/S0891-5849(00)00431-7.

Wang, J.F., Hori, K., Ding, J., Huang, Y., Kwan, P., Ladak, A., Tredget, E.E., 2011. Toll-like receptors expressed by dermal fibroblasts contribute to hypertrophic scarring. J. Cell. Physiol. https://doi.org/10.1002/jcp.22454.

Wang, Z.C., Zhao, W.Y., Cao, Y., Liu, Y.Q., Sun, Q., Shi, P., Cai, J.Q., Shen, X.Z., Tan, W. Q., 2020. The roles of inflammation in keloid and hypertrophic scars. Front. Immunol 11, 1– 10, 603187.

Xia, T., Li, J., Ren, X., Liu, C., Sun, C., 2021. Research progress of phenolic compounds regulating IL-6 to exert antitumor effects. Phytother. Res. 35, 6720–6734. https://doi.org/10.1002/ptr.7258.

Xue, H., McCauley, R.L., Zhang, W., Martini, D.K., 2000. Altered interleukin-6 expression in fibroblasts from hypertrophic burn scars. J. Burn Care Rehabil. https://doi.org/10.1097/00004630-200021020-00010.

You, J.Y., Kang, S.J., Rhee, W.J., 2021. Isolation of cabbage exosome-like nanovesicles and investigation of their biological activities in human cells. Bioact. Mater. 6, 4321–4332. https://doi.org/10.1016/j.bioactmat.2021.04.023.

Zhang, H., Wang, Z., Huang, J., Cao, J., Zhou, Y., Zhou, J., 2020. A novel thioredoxin-dependent peroxiredoxin (TPx-Q) plays an important role in defense against oxidative stress and is a possible drug target in babesia microti. Front. Vet. Sci 7, 1–11, 76.